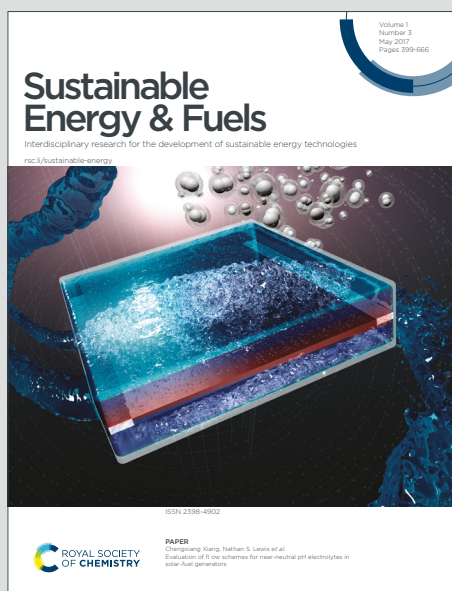


Sustainable Energy & Fuels

Interdisciplinary research for the development of sustainable energy technologies

Accepted Manuscript

This article can be cited before page numbers have been issued, to do this please use: A. Zhu, Z. Zou, A. Wang, C. Yu, Y. Yin and N. Li, *Sustainable Energy Fuels*, 2025, DOI: 10.1039/D5SE00888C.



This is an Accepted Manuscript, which has been through the Royal Society of Chemistry peer review process and has been accepted for publication.

Accepted Manuscripts are published online shortly after acceptance, before technical editing, formatting and proof reading. Using this free service, authors can make their results available to the community, in citable form, before we publish the edited article. We will replace this Accepted Manuscript with the edited and formatted Advance Article as soon as it is available.

You can find more information about Accepted Manuscripts in the [Information for Authors](#).

Please note that technical editing may introduce minor changes to the text and/or graphics, which may alter content. The journal's standard [Terms & Conditions](#) and the [Ethical guidelines](#) still apply. In no event shall the Royal Society of Chemistry be held responsible for any errors or omissions in this Accepted Manuscript or any consequences arising from the use of any information it contains.

ARTICLE

Received 00th January 20xx,
Accepted 00th January 20xx

DOI: 10.1039/x0xx00000x

Synthesis of jet fuel cycloalkane precursors with biomass-derived feedstocks over bimetallic Cu-Ni catalyst

Anran Zhu, Zhufan Zou, Aiqin Wang, Cong Yu, Yinghua Yin and Ning Li*

2,5-Bis(furan-2-ylmethyl)cyclopentan-1-one (FCFDH), a C₁₅ precursor for renewable jet fuel range cycloalkane and high-value electronic photolithography material, was selectively synthesized via a cascade aldol condensation/hydrogenation reaction of furfural and cyclopentanone under solvent-free conditions. Non-noble metal Cu and Ni modified MgAl-hydrotalcite (Cu₂Ni₁/MgAl-HT) was found to be an effective and stable catalyst for this reaction. Under the optimized conditions (423 K, 4 MPa H₂, 10 h), 97.0% cyclopentanone conversion and 82.0% carbon yield of FCFDH were achieved. Based on the characterization results, the presence of Ni and Cu species increased the acidity of MgAl-HT and formed Ni-Cu alloy particles with an average size of 2.33 nm during the preparation of catalyst. Both effects facilitate the aldol condensation of furfural and cyclopentanone and the formation of FCFDH by the selective hydrogenation of C=C bond.

Introduction

Due to the great social concern about sustainable development, the exploration and utilization of renewable energies have drawn a lot of attention. As the most abundant renewable carbon resource, biomass is a promising alternative for fossil energy in the production of fuels¹ and high-value chemicals.² Lignocellulose, which consists of cellulose, hemicellulose, and lignin, is particularly noteworthy due to its widespread availability, low cost, and carbon neutrality. Catalytic conversion is crucial for transforming lignocellulose into liquid fuels or specialty chemicals. This requires the development of efficient catalytic systems to optimize both the yield and selectivity of target products.

Furfural is an important platform compound that has been produced in industrial scale through the hydrolysis and dehydration of hemicellulose.³ After being hydrogenated under the aqueous phase conditions, furfural can be selectively converted to cyclopentanone.⁴ In the recent work of our group,⁵ cyclopentanone was selectively synthesized by the hydrogenolysis of xylose or hemicellulose extracted from raw biomass. In some recent literature, jet fuel range C₁₅ cycloalkane with high density and volumetric heat value was produced by the aldol condensation of cyclopentanone and furfural under the catalysis of NaOH,⁶ MgO-ZrO₂,⁷ KF/γ-Al₂O₃,⁷

Na-MgAlO_x,⁸ or acidic resins,⁹ followed by the hydrodeoxygenation (HDO). Owing to the cyclic carbon chain structure, cycloalkanes exhibit inherent ring strain compared to linear alkanes. This structural character endows cycloalkanes with higher density and volumetric energy density than those of conventional fuels. These physicochemical properties are highly desirable for advanced, high-performance fuels. However, the products from the aldol condensation of cyclopentanone with one or two furfural molecule(s) (*i.e.* 2-(2-furylmethylidene)cyclopentanone (FC) and 2,5-bis(2-furylmethylidene)cyclopentanone (FCF) in Scheme 1 are solid at room temperature. To facilitate the mass transfer, organic solvents are used in the HDO step. In real application, this will lead to higher energy consumption and lower efficiency. 2,5-Bis(furan-2-ylmethyl)cyclopentan-1-one (FCFDH) is an important intermediate for the manufacturing of high-precision photosensitive materials used in the semiconductor industry.¹⁰ In the conventional method, this compound can be produced by the selective hydrogenation of C=C bonds in FCF and exists as liquid state at room temperature. In the recent work of Wang *et al.*,¹¹ a one-pot process was developed for the direct synthesis of FCFDH with furfural and cyclopentanone by the cascade aldol condensation/hydrogenation under the co-catalysis of CaO and Pd/C. The FCFDH as obtained exists as a liquid at room temperature. Therefore, it can be directly used for the subsequent HDO under solvent-free conditions. Taking into consideration high price and low reserves of Pd, it is still imperative to develop non-noble metal catalyst.

In this work, a non-noble metallic Cu and Ni modified MgAl-hydrotalcite (Cu₂Ni₁/MgAl-HT) was found to be an effective and stable catalyst for the direct synthesis of FCFDH by a cascade aldol condensation/hydrogenation reaction with furfural and cyclopentanone under solvent-free conditions. To get deeper insight into the effect of Cu and Ni species in the

^a CAS Key Laboratory of Science and Technology on Applied Catalysis, Dalian Institute of Chemical Physics, Chinese Academy of Sciences, Dalian 116023, China.

^b University of Chinese Academy of Sciences, 19 A Yuquan Road, Shijingshan District, Beijing 100049, China.

^c State Key Laboratory of Catalysis, Dalian Institute of Chemical Physics, Chinese Academy of Sciences, Dalian 116023, China

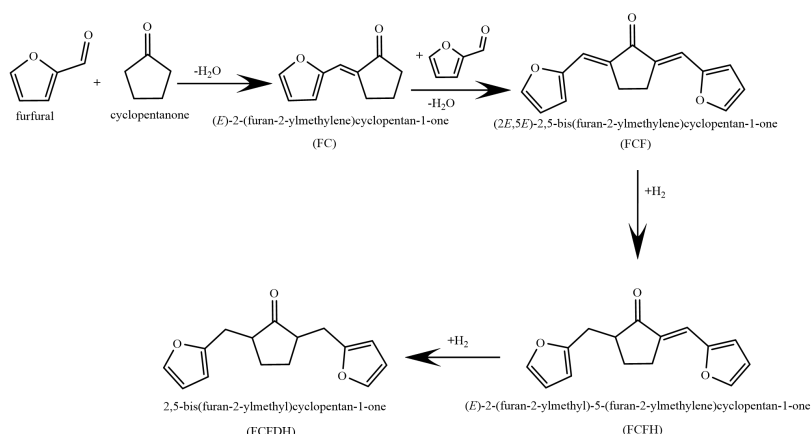
† Corresponding author: lining@dicp.ac.cn (Ning Li).

Electronic Supplementary Information (ESI) available: [details of any supplementary information available should be included here]. See DOI: 10.1039/x0xx00000x



reaction, the catalysts were characterized by a series of technologies. This study provides a sustainable and green

chemistry-compliant approach for synthesizing fuels or high value-added chemicals using furfural and its derivatives.



Scheme 1 Reaction route for the production of FCFDH from furfural and cyclopentanone.

Experimental

Chemicals

The $\text{Cu}(\text{NO}_3)_2 \cdot 3\text{H}_2\text{O}$, $\text{Ni}(\text{NO}_3)_2 \cdot 6\text{H}_2\text{O}$, $\text{Al}(\text{NO}_3)_3 \cdot 9\text{H}_2\text{O}$, $\text{Mg}(\text{NO}_3)_2 \cdot 6\text{H}_2\text{O}$, Na_2CO_3 and NaOH used in this work were purchased from Aladdin Bio-Chem Technology Ltd..

Catalyst preparation

Cu and Ni modified MgAl-hydrotalcite catalysts (denoted as $\text{Cu}_x\text{Ni}_y/\text{MgAl-HT}$, x and y means the theoretical atomic ratio of Cu and Ni) were prepared using a co-precipitation method. To facilitate the comparison, the total content of Cu and Ni in the catalyst were controlled as 5% by weight. Taking $\text{Cu}_2\text{Ni}_1/\text{MgAl-HT}$ as an example, 50 mL of the aqueous solution containing 0.08 mol Na_2CO_3 and 0.12 mol NaOH was slowly added dropwise to another aqueous solution containing 0.04 mol $\text{Mg}(\text{NO}_3)_2 \cdot 6\text{H}_2\text{O}$, 0.02 mol $\text{Al}(\text{NO}_3)_3 \cdot 9\text{H}_2\text{O}$, 0.0014 mol $\text{Cu}(\text{NO}_3)_2 \cdot 3\text{H}_2\text{O}$, and 0.0007 mol $\text{Ni}(\text{NO}_3)_2 \cdot 6\text{H}_2\text{O}$ under vigorous stirring. The pH of the obtained mixture was adjusted to 10 by a 3 mol L^{-1} NaOH solution. The mixture was kept at 338 K for 24 h, and the resulting slurry was filtered, washed with deionized water until the pH 7–8, and dried at 393 K for 12 h. Finally, the product was reduced at 773 K in a hydrogen flow (80 mL min^{-1}) for 4 h.

Characterization

X-ray diffraction (XRD) patterns of different catalysts were performed by a PANalytical X'Pert-Pro powder X-ray diffractometer using $\text{Cu K}\alpha$ monochromated radiation ($\lambda = 0.15418$ nm) at 40 V and 40 mA. N_2 physisorption of the catalysts was carried out by a Micromeritics ASAP 2010 apparatus. The elemental distribution of the catalysts was analyzed by scanning transmission electron microscopy (STEM) equipped with an energy dispersive X-ray spectroscopy (EDX) system. The basicity and acidity of the catalysts were characterized by CO_2 -chemisorption, CO_2 -TPD, NH_3 -

chemisorption and NH_3 -TPD using a Micromeritics AutoChem 2910 chemisorption analyzer. Typically, 0.1 g of catalyst was used for each test. Prior to the measurement, the catalyst was pretreated under He flow at 423 K for 0.5 h to remove adsorbed moisture and impurities, and then cooled to 353 K. After the baseline was stabilized, CO_2 (or NH_3) pulses were introduced until saturation adsorption was achieved. The adsorption signals were detected by a thermal conductivity detector (TCD), and the amounts of base (or acid) sites were calculated from the consumption of CO_2 (or NH_3). Subsequently, TPD experiments were carried out in the temperature range of 353–1173 K at a heating rate of 10 $\text{K}\cdot\text{min}^{-1}$ under He flow, and the desorption profiles were monitored by mass spectrometry (m/z 44 for CO_2 and m/z 15 for NH_3). The thermogravimetric–mass spectrometry (TG-MS) data of the catalyst were obtained using a TA Instruments SDT Q600 system coupled with an InProgress Instruments GAM 200 mass spectrometer (MS). For each measurement, 0.1 g of catalyst was loaded into the sample pan. The analyses were carried out under a flowing 20% O_2/N_2 mixture at a flow rate of 100 $\text{mL}\cdot\text{min}^{-1}$. During the test, the sample temperature was increased from 303 K to 1073 K at a heating rate of 10 $\text{K}\cdot\text{min}^{-1}$.

Activity test

The activity tests were carried out in a 50 mL stainless-steel batch reactor (Parr 5513 Stainless Steel, Parr Instrument). For each test, 10 mmol cyclopentanone, 20 mmol furfural, and 0.05 g catalysts were used. Before the tests, the reactor was purged with nitrogen for three times and charged with hydrogen to 4 MPa. After being heated at 423 K under stirring (at a rotation speed of 500 rpm) for 10 h and quenched to room temperature with cool water. The product was dissolved in 20 mL dichloromethane containing the internal standard of tridecane. The liquid products were analyzed by an Agilent 7890A gas chromatograph.

Conversion of the substrate (%) = (molar of the substrate consumed during activity test)/(molar of the substrate in the feedstock) \times 100%.



Carbon yield of specific product (%) = (molar of carbon in the specific product obtained in activity test)/(molar of carbon in the feedstock) \times 100%.

Result and discussion

MgAl-HT is a solid base catalyst that was often used in the aldol condensation of biomass derived carbonyl compounds.¹² In this work, it was reported for the first time that the modification of MgAl-HT catalyst with small amount of Cu or Ni species could significantly increase its activity for the condensation of furfural and cyclopentanone under hydrogen atmosphere (see Figure 1a and Figures S1-S5). Based on the analysis of products (see Figure 1b) and the Figures S1-S5 of supporting information, this phenomenon may be rationalized because the presence of Ni or Cu promoted the C=C bond in the FCF generated from the aldol condensation of furfural and cyclopentanone. As we know, the aldol condensation is a reversible reaction. From the point of view of reaction equilibrium, the saturation of C=C bonds in the FCF can prevent the retro aldol condensation. This could be one reason for the higher yields of C₁₅ oxygenates over the Cu/MgAl-HT and Ni/MgAl-HT catalysts. However, the carbon yields of FCFDH over the Cu/MgAl-HT and Ni/MgAl-HT catalysts were unsatisfactory.

When we used the bimetallic CuNi/MgAl-HT as the catalyst, evidently higher yields of FCFDH were achieved under the same reaction conditions (see Figure 1a, the carbon balances are shown in Figures S6). The advantage of the bimetallic catalyst is more evident when we use the Cu₂Ni₁/MgAl-HT as the catalyst (see Figure 1b). Over it, higher total yield of C₁₅ and C₁₀ oxygenates and lower yield of cyclopentanol than those over the other two bimetallic CuNi/MgAl-HT catalysts were achieved under the investigated reaction conditions. This is advantageous in real application. This phenomenon can be explained by the higher activity of the Cu₂Ni₁/MgAl-HT catalyst for the hydrogenation of C=C bonds in the FCF generated from the aldol condensation of furfural and cyclopentanone. As we know, the C₁₅ and C₁₀ oxygenates obtained in this work can be converted to jet fuel range C₁₅ and C₁₀ cycloalkanes. In contrast, the cyclopentane from the hydrodeoxygenation of cyclopentanol has low boiling point. Therefore, it can't be blended into the jet fuel.

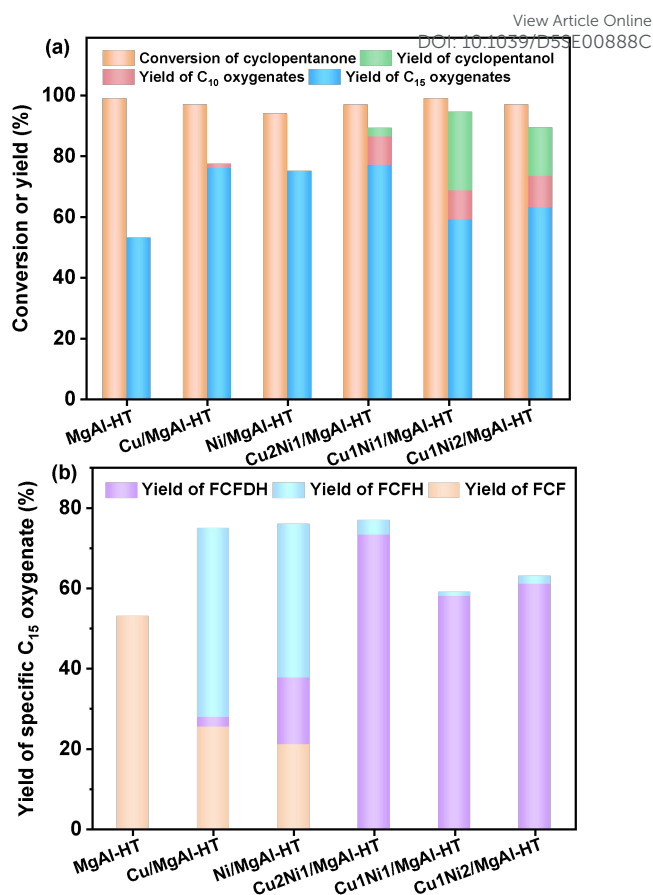


Figure 1. (a) Conversions of cyclopentanone and the yields of different products, and (b) the yield of the specific C₁₅ oxygenate over the different catalysts. Reaction conditions: 423 K, 4 MPa H₂, 10 h; 10 mmol cyclopentanone, 20 mmol furfural and 0.05 g catalyst were used in each test.

To gain deeper insight into the excellent performance of the Cu₂Ni₁/MgAl-HT, we characterized catalysts by a series of technologies. Based on the XRD patterns shown in Figure 2 and Figure 3, the precursors of Ni/MgAl-HT, Cu/MgAl-HT and Cu_xNi_y/MgAl-HT exhibited typical diffraction patterns at 2 θ angles of 11.7°, 23.4°, 34.5°, 39.6°, 60.7° and 62.2°, corresponding to the (003), (006), (012), (015), (018), (110) and (113) planes of LDHs (PDF #00-056-0956), respectively. Upon calcination at 773 K, the structure of LDHs was collapsed and converted to their corresponding highly dispersed mixed oxides. After the reduction at 773 K, major diffraction peaks at 2 θ angles of 37.2°, 43.2° and 62.8° were observed. These peaks can be assigned to the (111), (200) and (220) planes of Mg_{0.58}Al_{0.28}O (PDF #04-022-1660). No diffraction peaks corresponding to Cu or Ni species were observed, indicating that Cu and Ni species are highly dispersed on the surfaces of catalysts.



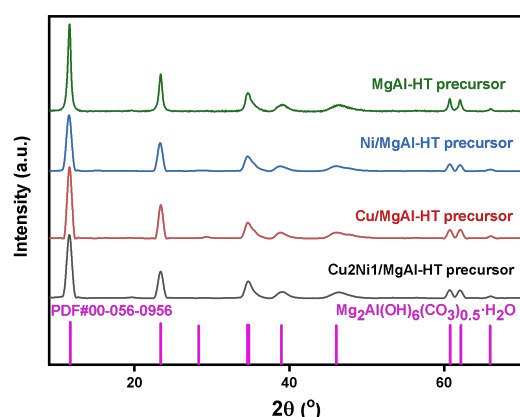


Figure 2. XRD patterns of the MgAl-HT, Ni/MgAl-HT, Cu/MgAl-HT and Cu₂Ni₁/MgAl-HT catalyst precursors.

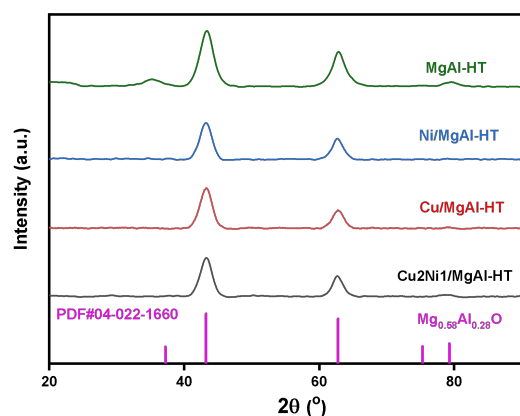


Figure 3. XRD patterns of the MgAl-HT, Ni/MgAl-HT, Cu/MgAl-HT and Cu₂Ni₁/MgAl-HT catalysts.

Subsequently, we also characterized the catalysts by N₂-physisorption. As shown in Figure 4 and Table 1, the N₂ adsorption-desorption isotherms of the catalysts exhibit a distinct hysteresis loop, characteristic of a type IV isotherm, indicating the presence of abundant mesoporous structures.¹⁹ It is worthy mention that the Cu₂Ni₁/MgAl-HT catalyst has evidently higher specific BET surface area (592 m² g⁻¹) than those of Cu/MgAl-HT (275 m² g⁻¹) and Ni/MgAl-HT (162 m² g⁻¹), which may be one reason for the higher activity of the Cu₂Ni₁/MgAl-HT catalyst for the hydrogenation of C=C bonds.

Table 1. Specific BET surface areas (*S*_{BET}), the pore volumes (*V*_t) and average pore sizes of MgAl-HT, Ni/MgAl-HT, Cu/MgAl-HT and Cu₂Ni₁/MgAl-HT catalysts.

Catalyst	<i>S</i> _{BET} (m ² g ⁻¹)	<i>V</i> _t (cm ³ g ⁻¹)	Average pore size (nm)
MgAl-HT	211	0.69	17.4
Ni/MgAl-HT	162	0.82	18.2
Cu/MgAl-HT	275	0.84	22.2
Cu ₂ Ni ₁ /MgAl-HT	592	1.91	20.9

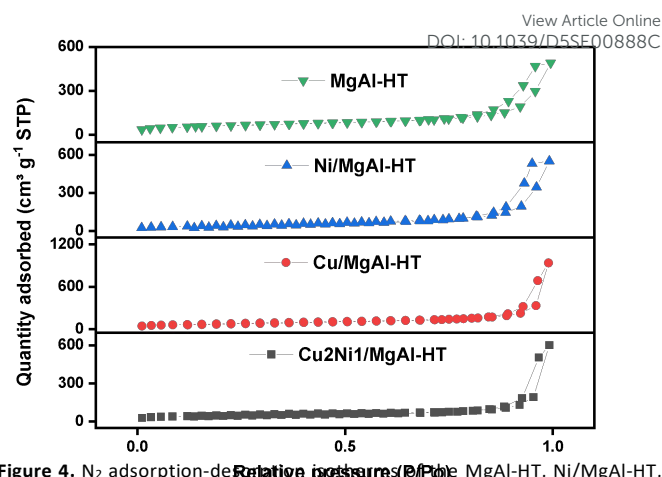


Figure 4. N₂ adsorption-desorption isotherms of MgAl-HT, Ni/MgAl-HT, Cu/MgAl-HT and Cu₂Ni₁/MgAl-HT catalysts.

The Cu₂Ni₁/MgAl-HT catalyst was also characterized by TEM. As shown in Figure 5a, the precursor of the Cu₂Ni₁/MgAl-HT catalyst exhibits a layered double hydroxide. This is consistent with the LDHs structure confirmed by XRD results. As shown in Figure 5e and Figures S7-S8, elemental mappings reveal that Mg, Al, Cu, and Ni species are highly dispersed. The elemental composition closely matches the theoretical values and the ones measured by ICP-OES analysis (Cu content: 2.9wt.%; Ni content: 1.3wt.%). After the reduction with hydrogen, the LDH framework collapsed and transformed into a mixed oxide phase. Remarkably, the MgAl-HT support effectively inhibited the sintering of metal particles, preserving high dispersion of metal nanoparticles with an average size of 2.33 nm (Figure 5b). As shown in Figure 5f, elemental mapping further validated the uniform distribution of metallic species. As shown in Figures 5c and 5d, isolated Ni nanoparticles displayed a lattice spacing of 0.202 nm, corresponding to the (111) plane of metallic Ni. Cu particles exhibited a characteristic (111) spacing of 0.208 nm. Bimetallic CuNi alloy domains were identified via a distinct (111) lattice spacing of 0.207 nm, intermediate between pure Cu and Ni values. The MgAl-HT support has a (200) plane spacing of 0.209 nm, matching XRD reference (PDF #04-022-1660). Besides, the MgAl-HT support and Ni (or Cu) species were closely interacted, forming a homogeneous boundary due to their close ionic radius and lattice matching between (200) plane of Mg_{0.58}Al_{0.28}O and (111) plane of Ni/Cu (Mg_{0.58}Al_{0.28}O: 0.209 nm, Ni: 0.202 nm, Cu: 0.208 nm). In Figure 5d, the Cu and Ni species were not directly observed. We believe that the majority of Cu species on the Cu₂Ni₁/MgAl-HT catalyst are strongly bound to either Ni and MgAl-HT support, forming a dilute CuNi alloy and Cu-modified MgAlO species. The strong interaction between the CuNi alloy particles and MgAl-HT support, driven by their similar ionic radii and lattice matching, creates a homogeneous boundary that inhibits metal particle aggregation, thus maintaining high activity in the hydrogenation of C=C bonds.



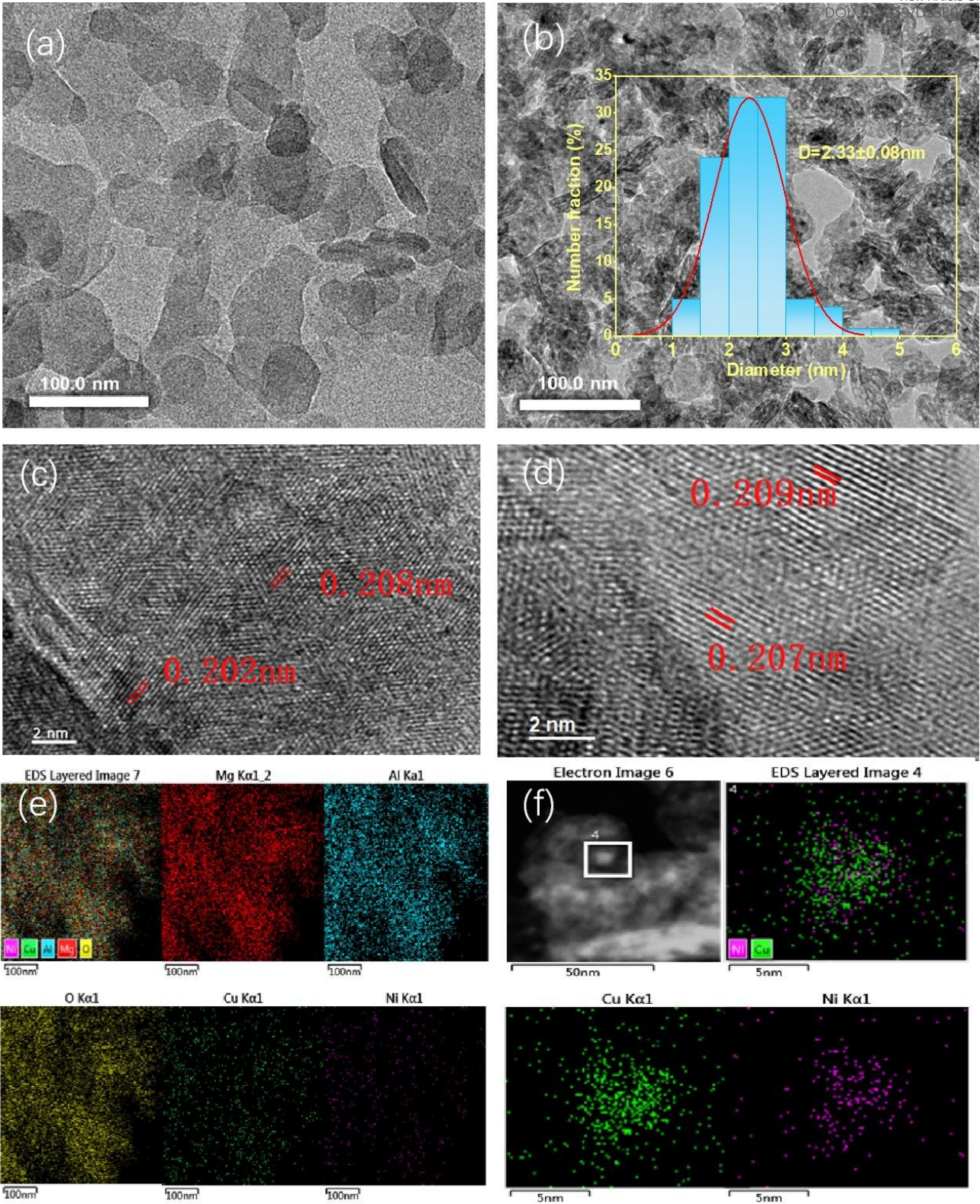


Figure 5. TEM images and the EDS elemental mappings of the Cu₂Ni₁/MgAl-HT precursors (a and e) and the Cu₂Ni₁/MgAl-HT catalyst (b, c, d and f).



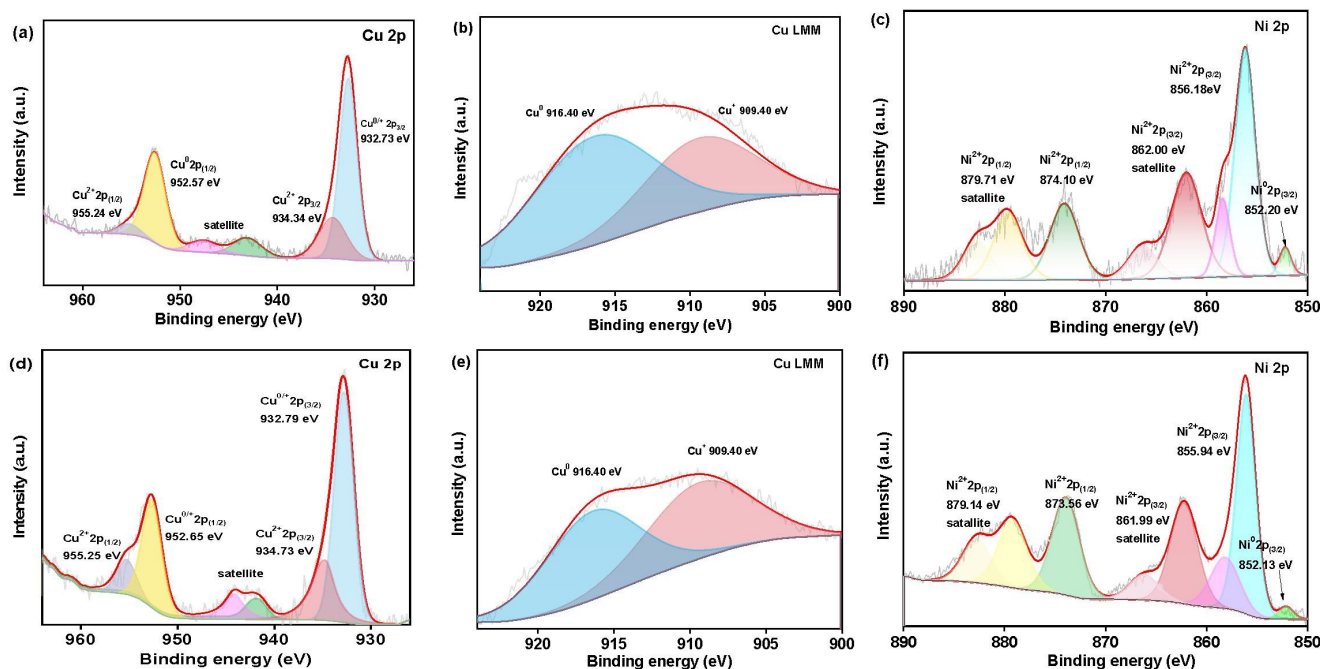


Figure 6. XPS spectra of (a–c) Cu 2p, Cu–LMM, and Ni 2p for Cu₂Ni₁/MgAl-HT, (d, e) Cu 2p and Cu–LMM for Cu/MgAl-HT, and (f) Ni 2p for Ni/MgAl-HT catalysts.

To discriminate the chemical states of Cu and/or Ni species, the catalysts were characterized by XPS (see Figure S9). In the spectra of Cu 2p (see Figures 6a and 6d), four distinct peaks were resolved at about 955.24 eV, 952.57 eV, 934.34 eV and 932.73 eV. These peaks can be attributed to the Cu 2p_{1/2} and Cu 2p_{3/2} signals of Cu²⁺, Cu⁰ or Cu⁺ species, respectively.¹³ The Cu²⁺ satellite peaks were also observed at around 945 eV. Figures 6b and 6e illustrated the Cu LMM Auger electron spectra that were used to distinguish Cu⁰ and Cu⁺ by deconvoluting the broad signal into two overlapping peaks at 916.40 eV and 909.40 eV, referring to Cu⁰ and Cu⁺ species, respectively.¹³ Based on the normalized areas of the corresponding featured peaks, the individual contents of Cu species with different valence states were quantified. The percentages of Cu⁰, Cu⁺, and Cu²⁺ species are summarized in Table 2. Based on Figures 6b and 6e, the Cu₂Ni₁/MgAl-HT and Cu/MgAl-HT contain Cu in three different oxidation states. The introduction of Ni species significantly increases the proportion of Cu⁰ and Cu⁺ on the catalyst surface. For the Cu₂Ni₁/MgAl-HT catalyst, approximately 25% of the Cu²⁺ species has strong interaction with Mg²⁺ or Ni²⁺ species, which makes them resistant to reduction under the given conditions, or from the surface reoxidation of metallic Cu particles during *ex-situ* measurements. Meanwhile, around 40% of Cu species exist as Cu⁰, which are almost atomically dispersed in the presence of metallic Ni. The remaining 35% of Cu species are present as Cu⁺, predominantly located at the interface between Cu⁰ and Cu²⁺/Mg²⁺.

In Figure 6c, five peaks at 879.71 eV, 874.10 eV, 862.00 eV, 856.18 eV and 852.20 eV were detected in the Ni 2p spectra of Cu₂Ni₁/MgAl catalyst. According to literature,¹⁴ these

peaks should be ascribed to Ni 2p_{1/2} satellite peak, Ni²⁺ 2p_{1/2}, Ni 2p_{3/2} satellite peak, Ni²⁺ 2p_{3/2} and Ni⁰ 2p_{3/2}, respectively. Accordingly, the Ni²⁺ and Ni⁰ species were concomitant on the surface of all samples. A certain amount of Ni²⁺ species originated either from the encapsulation effect, where Ni species interacted strongly with MgO(Al₂O₃) and were hardly reduced to metallic Ni or from the surface reoxidation of metallic Ni particles during the *ex-situ* measurements.

Compared with the Ni/MgAl-HT catalyst, the Ni 2p_{1/2} and 2p_{3/2} signals of the Cu₂Ni₁/MgAl-HT catalyst shift to higher binding energies (see Figure 6f). In contrast, the Cu 2p_{1/2} and 2p_{3/2} signals of Cu₂Ni₁/MgAl-HT shift to lower binding energies (see Figures 6a and 6d). These observations suggest that there is a strong interaction between the Cu and Ni species in the Cu₂Ni₁/MgAl-HT catalyst, leading to the transfer of electrons from Ni to Cu. The introduction of Ni effectively modulates the valence state distribution of Cu species, enhancing the ability to dissociate H₂, thereby improving hydrogenation activity. Additionally, it optimizes the interaction between Cu⁺ and Cu²⁺, refining the interfacial structure to facilitate hydrogen activation and transfer. These Cu species act as a dynamic reservoir for hydrogen adsorption/desorption processes, thereby promoting efficient hydrogen transfer. This optimization not only enhances hydrogen mobility on the catalyst surface but also improves the stability of Cu species, reducing the risk of sintering or deactivation.¹⁵

As shown in Figure S10 and Table 2, O 1s core level depicted two distinct peaks at 530.7 eV and 532.4 eV, which should be assigned to strong base sites of lattice oxygen (O_{latt}) and weak base sites of adsorbed oxygen, respectively. Compared with the



Ni/MgAl-HT catalyst, the percentage of O_{latt} of the Cu2Ni1/MgAl-HT catalyst was evidently higher (43.5% vs. 29.4%). This can be rationalized because the dehydration of hydroxyl oxygen in the presence of Cu species, which increased the strength of base sites for condensation reactions.¹⁶

DOI: 10.1039/D5SE00888C

Table 2. Surface atomic percentages of different Cu species and O species over the Ni/MgAl-HT, Cu/MgAl-HT, and Cu2Ni1/MgAl-HT catalysts, as determined from the normalized peak areas in the XPS spectra.

Catalyst	Surface atomic percentages of different Cu species (%)			Surface atomic percentages of different O species (%)	
	Cu ⁰	Cu ⁺	Cu ²⁺	O _{latt}	O _{ads}
Ni/MgAl-HT	--	--	--	29.4	70.6
Cu/MgAl-HT	29.9	33.4	36.7	45.2	54.8
Cu2Ni1/MgAl-HT	39.9	34.4	25.7	43.5	56.5

Based on the H₂-TPR profiles shown in Figure 7, the reduction temperature of the Cu2Ni1/MgAl-HT catalyst is higher than that of the Cu/MgAl-HT catalyst. Meanwhile, it is also lower than that of the Ni/MgAl-HT catalyst. These results further confirm the strong interactions between Cu and Ni species in the Cu2Ni1/MgAl-HT system. The H₂-TPR profiles of Cu2Ni1/MgAl-HT and Cu/MgAl-HT catalysts reveal two main reduction peaks. The peak at around 443 K corresponds to the reduction of highly dispersed CuO nanoparticles to Cu⁰, while the peak at around 620 K represents the reduction of larger CuO particles. Compared with the Cu/MgAl-HT catalyst, the peak at around 620 K in the profile of the Cu2Ni1/MgAl-HT catalyst shifts to a lower temperature, which indicates that the presence of Ni increases the reducibility of Cu species.

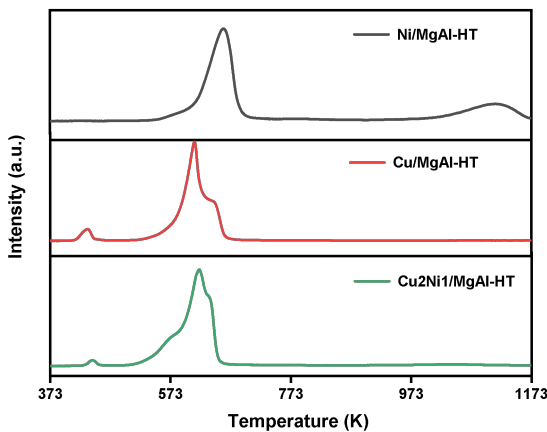


Figure 7. H₂-TPR profiles of the Ni/MgAl-HT, Cu/MgAl-HT and Cu2Ni1/MgAl-HT catalysts.

Furthermore, we also studied the basicity and acidity of the MgAl-HT, Cu/MgAl-HT, Ni/MgAl-HT and Cu2Ni1/MgAl-HT catalysts by CO₂-chemisorption and NH₃-chemisorption. From the results illustrated in Table 3, the base site concentrations of Cu/MgAl-HT, Ni/MgAl-HT and Cu2Ni1/MgAl-HT are lower than that of MgAl-HT. However, the acid site concentrations of Cu/MgAl-HT, Ni/MgAl-HT and Cu2Ni1/MgAl-HT are higher than that of MgAl-HT. This phenomenon is more evident for the Cu2Ni1/MgAl-HT. In the previous work of Corma *et al.*,¹⁷ it was suggested that acid sites can activate the carbonyl group by

polarizing the C=O bond and make the carbonyl group more electrophilic, which is favorable in aldol condensation. Based on these results, we believe that the relatively higher acidity of Cu2Ni1/MgAl-HT may be one reason for its excellent performance in the condensation of furfural and cyclopentanone. We also characterized these catalysts by CO₂-TPD and NH₃-TPD. Based on the results illustrated in Figures S11 and S12, no evident relationship was observed between the base strength (or acid strength) and their performance in the condensation of furfural and cyclopentanone.

Table 3. Base site and acid site concentrations of the investigated catalysts measured by CO₂-chemisorption and NH₃-chemisorption.

Catalyst	Base site concentration (μmol g ⁻¹)	Acid site concentration (μmol g ⁻¹)
MgAl-HT	111.7	51.2
Ni/MgAl-HT	54.6	187.2
Cu/MgAl-HT	87.1	177.2
Cu2Ni1/MgAl-HT	64.3	260.9

After further optimization of reaction temperature and reaction time (see Figures 8-9 and Figures S13–S14), 82.0% carbon yield of FCFDH was achieved over the Cu2Ni1/MgAl-HT catalyst after the reaction was carried out at 423 K, 4 MPa H₂ for 10 h. Taking into account the cyclopentanone conversion and the selectivity of FCFDH in the products, we believe that they are the optimal reaction conditions for the production of FCFDH over the Cu2Ni1/MgAl-HT catalyst. It was worth mentioning that the activity of the Cu2Ni1/MgAl-HT catalyst decreased after it was used in the activity test (see Figure S16). According to the results of N₂-physisorption and CO₂-chemisorption (see Table S1), evident decreases in the specific BET surface area, pore volume, average pore size and the amount of base sites were observed after the Cu2Ni1/MgAl-HT catalyst was used for the activity test, which may be the reason for the lower activity of spent Cu2Ni1/MgAl-HT catalyst. Based on thermogravimetric analysis (TGA) of the used Cu2Ni1/MgAl-HT catalyst (see Figure S17), these results can be rationalized by the carbon deposition generated during the reaction. As we know, furfural has high reactivity. Under the investigated conditions, it can be converted to furoic acid and furfuryl alcohol by Cannizzaro reaction. These compounds may react with base sites or form polymer on the surface of



Cu₂Ni/MgAl-HT catalyst, which should be the reason for the carbon deposition. As a solution to this problem, it was found that the Cu₂Ni/MgAl-HT catalyst can be regenerated by calcination and reduction (see Figure 10 and Figure S15). To fulfil the need of real application, we also checked the reusability of the Cu₂Ni/MgAl-HT catalyst. After each usage, the catalyst was thoroughly washed with methanol, calcined in

air at 737 K for 2 h and reduced in a hydrogen flow at 773 K for 4 h. As we expected, the Cu₂Ni/MgAl-HT catalyst was stable under the investigated conditions. No significant change in catalytic performance was observed during the five repeatedly usages (see Figure 10). Taking into consideration the high activity, good reusability, and low cost of the Cu₂Ni1/MgAl-HT, we think that it is a promising catalyst in future application.

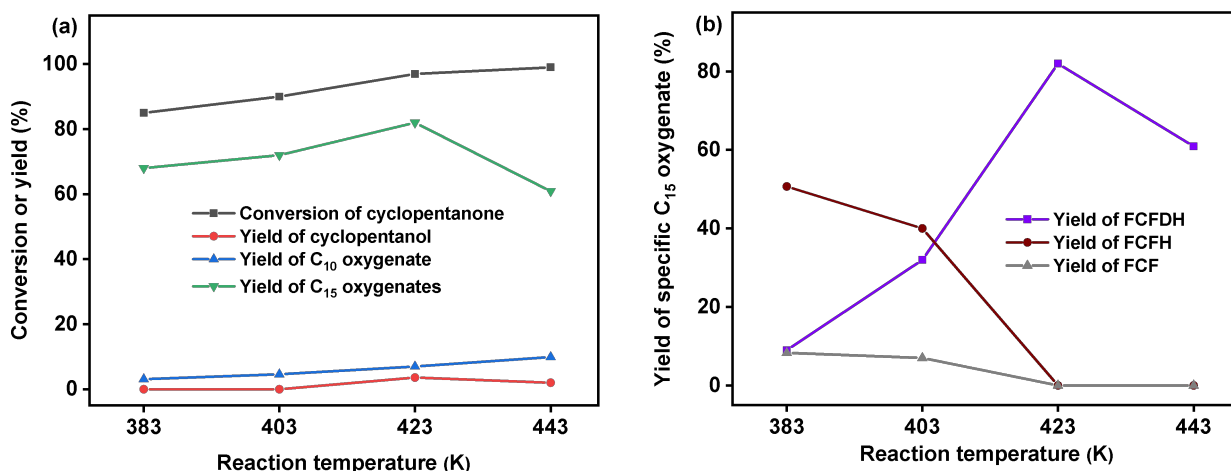


Figure 8. (a) Conversions of cyclopentanone and the yields of different products, and (b) yield of the specific C₁₅ oxygenate over the Cu₂Ni1/MgAl-HT catalyst as a function of reaction temperature. Reaction conditions: 4 MPa H₂, 10 h; 10 mmol cyclopentanone, 20 mmol furfural, 0.05 g Cu₂Ni1/MgAl-HT catalyst was used in each test.

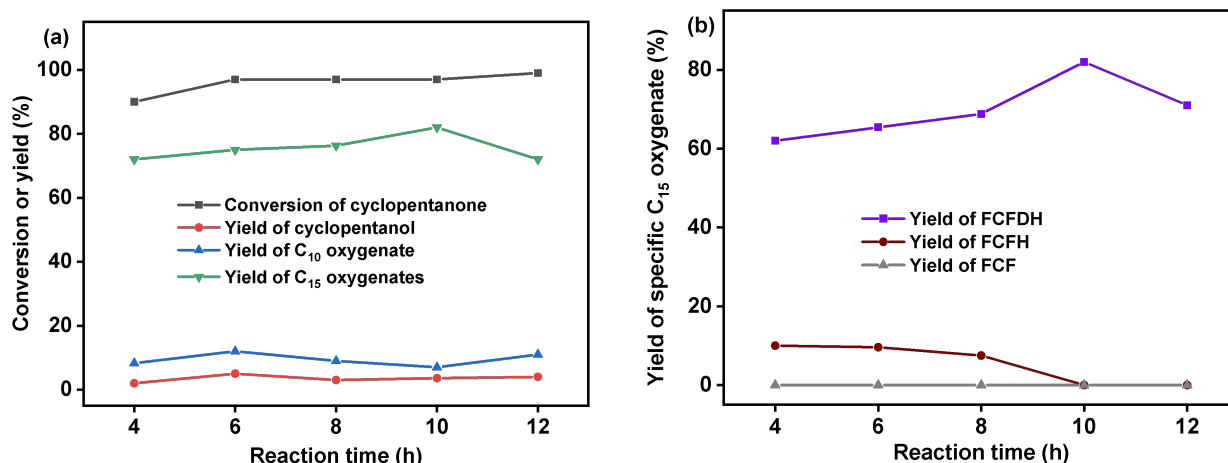


Figure 9. (a) Conversions of cyclopentanone and the yields of different products, and (b) yield of the specific C₁₅ oxygenate over the Cu₂Ni1/MgAl-HT catalyst as the function of reaction time. Reaction conditions: 423 K, 4 MPa H₂; 10 mmol cyclopentanone, 20 mmol furfural, 0.05 g Cu₂Ni1/MgAl-HT catalyst was used in each test.

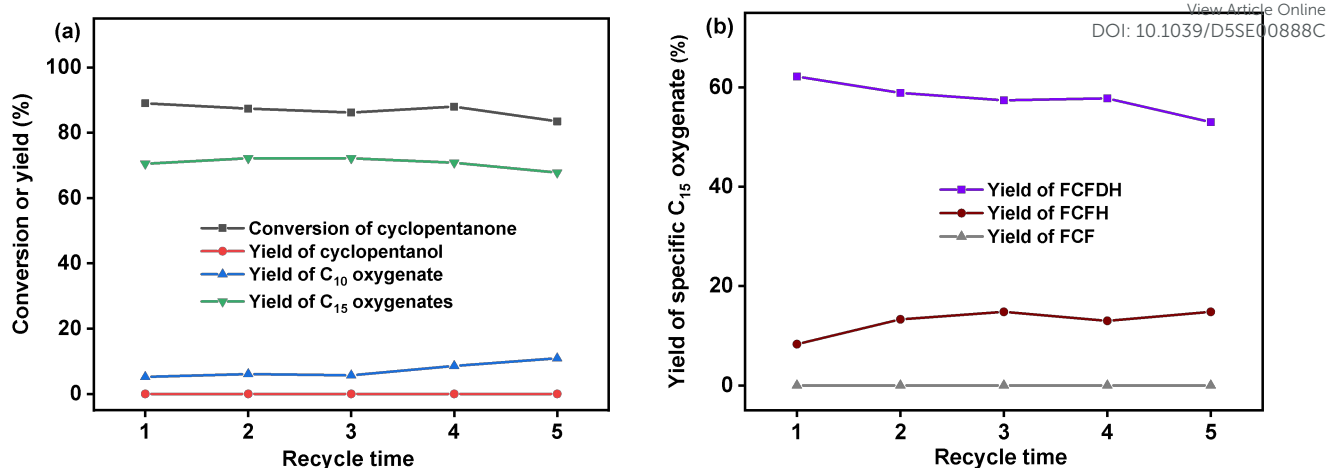


Figure 10. (a) Conversions of cyclopentanone and the yields of different products, and (b) yield of the specific C₁₅ oxygenate over the Cu₂Ni₁/MgAl-HT catalyst as the function of recycle time. Reaction conditions: 423 K, 4 MPa H₂, 1 h; 10 mmol cyclopentanone, 20 mmol furfural, 0.05 g Cu₂Ni₁/MgAl-HT catalyst was used in each test.

Conclusions

Bimetallic Cu₂Ni₁/MgAl-HT catalyst demonstrated excellent activity and stability for the direct synthesis of FCFDH by the cascade aldol condensation/hydrogenation reaction of furfural and cyclopentanone that can be derived from lignocellulose. Under optimized conditions (423 K, 4 MPa H₂, 10 h), high cyclopentanone conversion and good yield of FCFDH were achieved over the Cu₂Ni₁/MgAl-HT catalyst. Based on the characterization results, the introduction of Ni species led to the formation of CuNi alloy sites due to their similar ionic radii and lattice matching, which is favorable for the selective hydrogenation of C=C bonds in the FCF generated from the aldol condensation of furfural and cyclopentanone. Moreover, the modification of MgAl-HT with Cu and Ni also increased its acidity. Both effects led to the good performance of Cu₂Ni₁/MgAl-HT catalyst for the direct synthesis of FCFDH with furfural and cyclopentanone under the investigated conditions. This study provides valuable insights into the synthesis of jet-fuel precursors from furfural and cyclopentanone with non-noble metal bifunctional catalysts.

Conflicts of interest

There are no conflicts to declare.

Acknowledgements

This work was supported by National Natural Science Foundation of China (no. 22178335), DICP (Grant: DICP I202448).

Notes and references

- G. W. Huber, S. Iborra and A. Corma, *Chem. Rev.*, 2006, **106**, 4044-4098; G. Li, R. Wang, J. Pang, A. Wang, N. Li and T. Zhang, *Chem. Rev.*, 2024, **124**, 2889-2954; G. W. Huber, J. N. Chheda, C. J. Barrett and J. A. Dumesic, *Science*, 2005, **308**, 1446-1450; E. L.

- Kunkes, D. A. Simonetti, R. M. West, J. C. Serrano-Ruiz, C. A. Gartner and J. A. Dumesic, *Science*, 2008, **322**, 417-421; B. G. Harvey and R. L. Quintana, *Energy Environ. Sci.*, 2010, **3**, 352-357; A. Corma, O. de la Torre, M. Renz and N. Villandier, *Angew. Chem., Int. Ed.*, 2011, **50**, 2375-2378; P. Anbarasan, Z. C. Baer, S. Sreekumar, E. Gross, J. B. Binder, H. W. Blanch, D. S. Clark and F. D. Toste, *Nature*, 2012, **491**, 235-239; A. Corma, O. de la Torre and M. Renz, *Energy Environ. Sci.*, 2012, **5**, 6328-6344; J. Q. Bond, A. A. Upadhye, H. Olcay, G. A. Tompsett, J. Jae, R. Xing, D. M. Alonso, D. Wang, T. Zhang, R. Kumar, A. Foster, S. M. Sen, C. T. Maravelias, R. Malina, S. R. H. Barrett, R. Lobo, C. E. Wyman, J. A. Dumesic and G. W. Huber, *Energy Environ. Sci.*, 2014, **7**, 1500-1523; Q.-N. Xia, Q. Cuan, X.-H. Liu, X.-Q. Gong, G.-Z. Lu and Y.-Q. Wang, *Angew. Chem., Int. Ed.*, 2014, **53**, 9755-9760; Q. Xia, Z. Chen, Y. Shao, X. Gong, H. Wang, X. Liu, S. F. Parker, X. Han, S. Yang and Y. Wang, *Nat. Commun.*, 2016, **7**, 11162.
- M. J. Climent, A. Corma and S. Iborra, *Chem. Rev.*, 2011, **111**, 1072-1133; A. Wang and T. Zhang, *Acc. Chem. Res.*, 2013, **46**, 1377-1386; C. Li, X. Zhao, A. Wang, G. W. Huber and T. Zhang, *Chem. Rev.*, 2015, **115**, 11559-11624; S. Shylesh, A. A. Gokhale, C. R. Ho and A. T. Bell, *Acc. Chem. Res.*, 2017, **50**, 2589-2597; C. Luo, S. Wang and H. Liu, *Angew. Chem., Int. Ed.*, 2007, **46**, 7636-7639; H. Liu, T. Jiang, B. Han, S. Liang and Y. Zhou, *Science*, 2009, **326**, 1250-1252; T. P. Vispute, H. Y. Zhang, A. Sanna, R. Xiao and G. W. Huber, *Science*, 2010, **330**, 1222-1227; Y. Liu, C. Luo and H. C. Liu, *Angew. Chem., Int. Ed.*, 2012, **51**, 3249-3253; Y. L. Wang, W. P. Deng, B. J. Wang, Q. H. Zhang, X. Y. Wan, Z. C. Tang, Y. Wang, C. Zhu, Z. X. Cao, G. C. Wang and H. L. Wan, *Nat. Commun.*, 2013, **4**, 2141; W. Deng, Y. Wang, S. Zhang, K. M. Gupta, M. J. Hülsey, H. Asakura, L. Liu, Y. Han, E. M. Karp, G. T. Beckham, P. J. Dyson, J. Jiang, T. Tanaka, Y. Wang and N. Yan, *Proc. Natl. Acad. Sci. U.S.A.*, 2018, **115**, 5093-5098; W. Deng, L. Yan, B. Wang, Q. Zhang, H. Song, S. Wang, Q. Zhang and Y. Wang, *Angew. Chem., Int. Ed.*, 2021, **60**, 4712-4719; Q. Meng, J. Yan, R. Wu, H. Liu, Y. Sun, N. Wu, J. Xiang, L. Zheng, J. Zhang and B. Han, *Nat. Commun.*, 2021, **12**, 4534; K. Zhang, Q. Meng, H. Wu, J. Yan, X. Mei, P. An, L. Zheng, J. Zhang, M. He and B. Han, *J. Am. Chem. Soc.*, 2022, **144**, 20834-20846; A. Osatiashtiani, A. F. Lee, D. R. Brown, J. A. Melero, G. Morales and K. Wilson, *Catal. Sci. Technol.*, 2014, **4**, 333-342; M. T. Reche, A. Osatiashtiani, L. J.



- Durndell, M. A. Isaacs, A. Silva, A. F. Lee and K. Wilson, *Catal. Sci. Technol.*, 2016, **6**, 7334-7341.
3. J.-P. Lange, E. van der Heide, J. van Buijtenen and R. Price, *ChemSusChem*, 2012, **5**, 150-166.
 4. M. Hronec and K. Fulajtarova, *Catal. Commun.*, 2012, **24**, 100-104; R. Fang, H. Liu, R. Luque and Y. Li, *Green Chem.*, 2015, **17**, 4183-4188; X.-L. Li, J. Deng, J. Shi, T. Pan, C.-G. Yu, H.-J. Xu and Y. Fu, *Green Chem.*, 2015, **17**, 1038-1046; G. S. Zhang, M. M. Zhu, Q. Zhang, Y. M. Liu, H. Y. He and Y. Cao, *Green Chem.*, 2016, **18**, 2155-2164; Y. Yang, Z. Du, Y. Huang, F. Lu, F. Wang, J. Gao and J. Xu, *Green Chem.*, 2013, **15**, 1932-1940.
 5. Z. Yu, Z. Zou, R. Wang, G. Li, A. Wang, Y. Cong, T. Zhang and N. Li, *Angew. Chem., Int. Ed.*, 2023, **62**, e202300008; Z. Zou, Z. Yu, W. Guan, Y. Liu, Y. Yao, Y. Han, G. Li, A. Wang, Y. Cong, X. Liang, T. Zhang and N. Li, *Nat. Commun.*, 2024, **15**, 3723.
 6. R. Baldenhofer, J.-P. Lange, S. R. A. Kersten and M. P. Ruiz, *ACS Sustainable Chem. Eng.*, 2025, **13**, 681-691.
 7. L. Ao, W. Zhao, Y. S. Guan, D. K. Wang, K. S. Liu, T. T. Guo, X. Fan and X. Y. Wei, *RSC Adv.*, 2019, **9**, 3661-3668.
 8. Q. Liu, X. Zhang, Q. Zhang, Q. Liu, C. Wang and L. Ma, *Energy Fuels*, 2020, **34**, 7149-7159.
 9. W. Wang, X. Ji, H. Ge, Z. Li, G. Tian, X. Shao and Q. Zhang, *RSC Adv.*, 2017, **7**, 16901-16907.
 10. J. Li, Y. Hao, M. Zhong, L. Tang, J. Nie and X. Zhu, *Dyes and Pigments*, 2019, **165**, 467-473; F. Dumur, *Catalysts*, 2023, **13**, 493.
 11. W. Wang, S. Y. Sun, F. G. Han, G. Y. Li, X. Z. Shao and N. Li, *Catalysts*, 2019, **9**, 11.
 12. S. Shao, W. Dong, X. Li, H. Zhang, R. Xiao and Y. Cai, *Journal of Cleaner Production*, 2020, **250**, 119459.
 13. Q. Wang, J. Feng, L. Zheng, B. Wang, R. Bi, Y. He, H. Liu and D. Li, *ACS Catal.*, 2020, **10**, 1353-1365.
 14. M.-M. Millet, G. Algara-Siller, S. Wrabetz, A. Mazheika, F. Girgsdies, D. Teschner, F. Seitz, A. Tarasov, S. V. Levchenko, R. Schlögl and E. Frei, *J. Am. Chem. Soc.*, 2019, **141**, 2451-2461; T. X. Nguyen, J. Patra, J.-K. Chang and J.-M. Ting, *J. Mater. Chem. A*, 2020, **8**, 18963-18973; P. S. Bagus, C. J. Nelin, C. R. Brundle, B. V. Crist, E. S. Ilton, N. Lahiri and K. M. Rosso, *Inorganic Chemistry*, 2022, **61**, 18077-18094.
 15. M. Wang, H. Chen, M. Wang, J. Wang, Y. Tuo, W. Li, S. Zhou, L. Kong, G. Liu, L. Jiang and G. Wang, *Angew. Chem., Int. Ed.*, 2023, **62**, e202306456; M. Gao, Z. Wang, Z. Liu, Y. Huang, F. Wang, M. Wang, S. Yang, J. Li, J. Liu, H. Qi, P. Zhang, X. Lu and X. Feng, *Adv. Mater.*, 2023, **35**, 2305575; S. Poulston, P. M. Parlett, P. Stone and M. Bowker, *Surface and Interface Analysis*, 1996, **24**, 811-820.
 16. X. Zhou, C. Luo, M. Luo, Q. Wang, J. Wang, Z. Liao, Z. Chen and Z. Chen, *Chem. Eng. J.*, 2020, **381**, 122587.
 17. M. a. J. Climent, A. Corma, S. Iborra and A. Velty, *J. Mol. Catal. A: Chem.*, 2002, **182-183**, 327-342.



Data availability statements:

[View Article Online](#)
DOI: 10.1039/D5SE00888C

The data supporting this article have been included as part of the ESI.†

